FULL PAPER

Triggering Mechanism for DNA Electrical Conductivity: Reversible Electron Transfer between DNA and Iron Oxide Nanoparticles

Massimiliano Magro, Davide Baratella, Petr Jakubec, Giorgio Zoppellaro, Jiri Tucek, Claudia Aparicio, Rina Venerando, Geppo Sartori, Federica Francescato, Fabio Mion, Nadia Gabellini, Radek Zboril, and Fabio Vianello**

A new category of iron oxide nanoparticles (surface active maghemite nanoparticles (SAMNs, γ-Fe_2O_3)) allows the intimate chemical and electrical contact with DNA by direct covalent binding. On these basis, different DNA-nanoparticle architectures are developed and used as platform for studying electrical properties of DNA. The macroscopic 3D nanobioconjugate, constituted of 5% SAMNs, 70% water, and 25% DNA, shows high stability, electrochemical reversibility and, moreover, electrical conductivity (70–80 Ω cm^{-1}). Reversible electron transfer at the interface between nanoparticles and DNA is unequivocally demonstrated by Mössbauer spectroscopy, which shows the appearance of Fe(II) atoms on nanoparticles following nanobioconjugate formation. This represents the first example of permanent electron exchange by DNA, as well as, of DNA conductivity at a macroscopic scale. Finally, the most probable configuration of the binding is tentatively modeled by density functional theory (DFT/UBP86/6-31+G*), showing the occurrence of electron transfer from the organic orbitals of DNA to surface exposed Fe(III) on nanoparticles, as well as the generation of defects (holes) on the DNA bases. The unequivocal demonstration of DNA conduction provides a new perspective in the five decades long debate about electrical properties of this biopolymer, further suggesting novel approaches for DNA exploitation in nanoelectronics.

1. Introduction

The use of DNA molecules as scaffolds, supports, and templates has inspired diverse branches of the modern nanobioscience. The current technological applications of DNA span from the use of nucleic acid templates to activate enzyme cascades,[1] and self-assembly of nanoscale nucleic acid building blocks into mesoscale structures,[2] to self-organization of supramolecular DNA nanostructures acting as molecular nanomachines.[3] DNA has been proposed as biological template for the assembly of nanoelectronic devices and nanocircuits.[4] Moreover, DNA has been extensively investigated for the development of field-effect transistors,[5] chemical and biological sensors,[6] and nanodiodes.[7] From the structural perspective, the DNA molecule can be considered as a nanowire, with diameter of 2 nm, featuring long well-defined polymeric sequences decorated by functional groups.[8] The understanding of the conducting properties of DNA molecules has been a scientific challenge for more than 50 years. The possible charge transfer between electron donors and acceptors through DNA, obtained from solution chemistry experiments,[9] stimulated a series of direct electron transfer measurements aimed at the development of high-tech applications, ranging from band-gap insulators to effective molecular wires.[10] Yet, understanding the electrical conduction properties of such complicated aperiodic polyelectrolyte system remains a major scientific problem.[11] The prevailing DNA architecture, the double helix, possess well stacked, nearly parallel bases, with overlapping π-electron systems[10] and, thus, can be a good candidate for long-range charge transfer.[12] Notwithstanding experimental findings and theoretical interpretations have spurred intense debate over the electrical properties of DNA, the electronic properties of DNA still remain controversial, and the nature of the carriers responsible for DNA electrical conductivity is still under investigation. It has been demonstrated that both vacancies and electrons can migrate through the DNA helix over distances,[13] as well as, results indicate that correlation effects are probably responsible

Dr. M. Magro, Dr. D. Baratella, Dr. F. Francescato, F. Mion, Prof. F. Vianello
Department of Comparative Biomedicine and Food Science
University of Padova
Legnaro 35044, Italy
E-mail: fabio.vianello@unipd.it
Dr. P. Jakubec, Dr. G. Zoppellaro, Dr. J. Tucek, Dr. C. Aparicio, Prof. R. Zboril
Regional Centre of Advanced Technologies and Materials
Department of Physical Chemistry
Faculty of Science
Palacky University
Olomouc 779 00, Czech Republic
E-mail: radek.zboril@upol.cz
Dr. G. Sartori
Department of Biomedical Sciences
University of Padova
Padova 35131, Italy
Dr. R. Venerando, Dr. N. Gabellini
Department of Molecular Medicine
University of Padova
Padova 35131, Italy
DOI: 10.1002/adfm.201404372

for large hopping distances in DNA samples.[14] Consequently, electrochemistry of nucleic acids and DNA modified electrodes may provide valuable insights into charge transfer processes and could be exploited in the design of electrochemical DNA-based biosensors. It should be mentioned that a general critical issue in bioelectrochemistry is the creation of electrical contact between redox-active sites of biological molecules and electrodes,[15] therefore, in the particular case of DNA, an electrical contact between the biopolymer and redox active sites represents a challenging target. Up to authors knowledge, DNA-based conductive nanowires have been fabricated by conjugating metallic,[16] semiconducting,[17] and polymeric[18] nanomaterials to DNA, mainly via electrostatic interactions, and no electrochemical applications were reported in literature exploiting redox reactions directly at DNA–metal oxide interface. Therefore, in the present work, surface active maghemite nanoparticles (SAMNs)[19] were used as electroactive support for DNA immobilization. The peculiar surface properties of SAMNs were exploited to achieve DNA immobilization. In this way, 1D, 2D DNA based self-assembled nanobioconjugates have been synthetized, leading to a significant improvement of electrochemical performances with respect to nonfunctionalized nanoparticles.

3D nanobioconjugates, in which SAMNs represented only 5.0% of the total conjugate, showed peculiar properties, rather than inherited directly from individual subunits and resulted in electrically conductive materials (70–80 Ω cm^{-1}). The nature of the intimate contact between DNA and crystalline iron oxide nanoparticles was characterized. Mössbauer spectroscopy highlighted the migration of electrons at the interface between DNA and maghemite nanoparticles, inferring the formation of Fe(II) in the nanobioconjugate. The occurrence of an electron transfer from DNA organic orbitals to surface exposed Fe(III) on nanoparticles as well as the generation of defects (holes) in the DNA bases was tentatively modeled by density functional theory (DFT/UBP86/6–31+G*) approach. DNA–SAMN hybrid superstructure may provide a new class of metamaterials, revealing new tailored electrochemical functionalities.

2. Results

The first part of the present study deals with the self-assembly process of one-, two- and three nanobioconjugates by covalent immobilization of DNA on SAMN surface. The peculiar behavior of SAMNs, being constituted of common maghemite, is due to their surface properties and, as already reported on an our previous papers,[20] experimental evidences suggested the presence of under-coordinated Fe(III) sites located at SAMN surface. Therefore, we exploited under-coordinated Fe(III) sites for DNA conjugation by simple incubation in water. For clarity, these complexes were considered as core–shell systems, namely SAMN@DNA. In this scenario, DNA molecules and maghemite nanoparticles represent the shell and the core, respectively. DNA molecules were distinguished by their length, expressed as number of bases or pairs of bases. As an example, six base long DNA has been called throughout DNA6b and the conjugate obtained by the immobilization of DNA6b on SAMNs was named SAMN@DNA6b. The short length of this DNA molecule prevents the involvement of more than one nanoparticle in the conjugate formation, and thus leads to 1D nanobioconjugate. Conversely, long length molecules may indeed produce linear geometries with several nanoparticles coordinating the same DNA molecule, namely 2D nanobioconjugates.

The immobilization of DNA on nanoparticle surface was studied as a function of its concentration in solution, according to the Langmuir isotherm model.[21] Results on 1D and 2D nanobioconjugate formation are reported in Figure S3, Supporting Information. Nanoparticle loading and, as consequence, the final SAMN@DNA conjugate architecture depend on DNA length (in the 500–15 000 bp range), and, at the same time, on SAMN concentration. In order to evaluate the length of the DNA region involved in the effective intimate chemical contact with SAMN surface, expressed as number of base pairs adsorbed on nanomaterial surface, an endonuclease digestion analysis was adopted.[22] In particular, genomic DNA (15 000 bp) displays the highest affinity for SAMNs and a wrapping mechanism, recalling the histone model, can be suggested (see the Supporting Information).[23] Finally, 2D SAMN@DNA complexes can be forced to organize into a macroscopic structure, namely a 3D nanobioconjugate or metamaterial.

2.1. 3D Nanobioconjugate (SAMN@DNA Metamaterial)

Due to their versatile surface chemistry, SAMNs can be a useful tool to create 3D DNA architectures, leading to macroscopic organization in a metamaterial, in which SAMNs behave as junction blocks. In this case, the chaotropic effect of perchloric acid (1 M) forced DNA based 2D nanoconjugates to collapse, leading to crosslinking into a 3D framework (see Methods in the Supporting Information).

In fact, as reported in the Supplementary Information section, a single DNA strand does not tend to wrap completely on a single nanoparticle, thus the biopolymer immobilization does not involve the complete saturation of under-coordinated iron sites on SAMN surface. As a consequence, portions of reactive SAMN surface are still available for further DNA binding. In addition, endonuclease digestion experiments showed that individual SAMNs are distanced by unbound oligonucleotide segments, namely linker DNA (see the Supporting Information). Therefore, these DNA linkers in 2D nanobioconjugates are potentially able to bind on the still available surface of SAMNs, belonging to other 2D nanobioconjugates, thus generating a cross-linked network. The novel macroscopic metamaterial, composed of SAMNs and DNA, was obtained with a yield of >99% with respect to the initial reactants (see **Figure 1**A).

The metamaterial, as prepared and isolated, appeared in the form of a brown sticky film, several tens of square centimeter wide, which was characterized by transmission electron microscopy (TEM) (see Figure 1B,C). TEM microscopy images indicated the presence of a DNA organic matrix, characterized by a lower electron density, encaging the iron oxide nanoparticles. SAMNs were evenly dispersed in the DNA matrix and presented only few macro aggregates, in comparison with conventional air dried samples.[24] Conversely, nanoparticles appeared organized in small clusters (Figure 1C), composed, in average

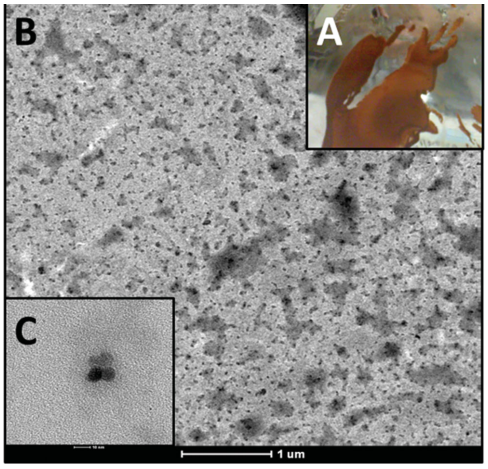

Figure 1. TEM images and photo of SAMN@DNA metamaterial. A) Photo image of SAMN@DNA metamaterial; B) low magnification TEM image of SAMN@DNA metamaterial; and C) high magnification TEM image of SAMN@DNA metamaterial.

by 4–5 nanoparticles. The distribution of SAMN clusters inside the DNA matrix in the metamaterial was estimated by dissecting TEM images into 1 μm^2 square areas and evaluating the cluster number in each area by NIH (National Institute of Health, USA) ImageJ software. In order to evidence a cluster position within the sample, a grayscale threshold was used. In addition, to exclude the interference of few larger aggregates, high electron-density areas > 120 nm^2 were excluded from the calculation. In Figure S9, Supporting Information, the distribution of identified SAMN clusters per μm^2 surface area is reported. It can be noted that 22.45 ± 5.57 (SD) SAMN clusters per μm^2, homogeneously distributed, were present in the metamaterial. The clusters observed by TEM could be interpreted as junction points, representing the aggregation of SAMNs and linker DNA segments belonging to different 2D nanobioconjugates. The average minimum distance between the SAMN clusters in the TEM image of the metamaterial was calculated by the "Nearest Neighbor Distances Calculation" plug-in software (see Figure S10, Supporting Information): it resulted of 107.8 ± 23.4 nm (SD, standard deviation). The average distance was not statistically different (Neuman–Keuls multiple comparison test at 0.05%) among all the analyzed 1 μm^2 areas, suggesting that SAMN clusters were evenly distributed within the organic matrix, leading to an amorphous metamaterial with characteristic periodicity and 3D organization, as a superstructure. Finally, the metamaterial resulted constituted of 25% DNA, 70% water, and SAMNs represented only the 5% of its total mass.

2.2. Electrochemical Characterization of SAMN@DNA Nanobioconjugates

In order to characterize the electrochemical behavior of the self-assembled SAMN@DNA materials, the nanobioconjugates were used to prepare modified carbon paste electrodes (CPEs). Tentatively, all CPEs were prepared by mixing 55% (w/w) graphite, 30% (w/w) silicone grease, and 15% (w/w) of the tested conjugate, as already reported.[19c,25] The CP modified electrodes were first characterized by Electrochemical Impedance Spectroscopy (EIS), as powerful tool for the study of electrode surface modifications. The impedance-plane plot (Nyquist diagrams), shown in Figure S4, Supporting Material is characterized by two distinct regions: (i) a semicircle at higher frequency, related to charge transfer resistance of the electrode/electrolyte interface, R_{ct}; (ii) A linear region defining a semiinfinite diffusion of species at the modified electrode (Warburg region). The model circuit used in this study was a typical Randles circuit.[26] The comparison of R_{ct} values determined for the unmodified CPEs with CPEs modified with 15% SAMNs showed that, in the presence of maghemite nanoparticles, a fourfold increase of electrode R_{ct} occurred (see Table S2, Supporting Information). CP electrodes modified with SAMN@DNA6bs showed very low R_{ct} values, and, considering that the biomolecule represented only 0.6% of the total conjugate weight, this indicates that DNA immobilization facilitates the electron transfer between the carbon paste matrix and maghemite nanoparticles. For all the produced SAMN@DNA conjugates, R_{ct} values were from 20 to 40 times lower than the electrode based on bare maghemite nanoparticles. Furthermore, the electrocatalytic behavior of SAMN@DNA modified CP electrodes was tested on a common electroactive substance, namely hydrogen peroxide (see Figure S6 inset, Supporting Information). The electrocatalytic performances of modified electrodes were evaluated by chronoamperometry in the presence of H_2O_2 at very low applied potentials and results are reported in Table S3, Supporting Information. The best electrochemical performances were observed with CP electrodes modified with SAMN@DNA1000bp complex (see Table S3, Supporting Information). In this case, the electrode sensitivity toward hydrogen peroxide was about 230% (about 60 nA μM^{-1} cm^{-2}) with respect to bare SAMNs, and a detection limit of 2×10^{-6} M H_2O_2 ($S/N = 3$), was determined. In addition, a novel application for H_2O_2 detection at very low concentrations can be proposed using simple SAMN@DNA modified CPEs. It should be emphasized that H_2O_2 can be electrochemically oxidized or reduced directly at ordinary solid electrodes. However, these processes are limited by slow electrode kinetics and high overpotential, which affect the sensing performances and may cause large interferences from other existing electroactive species in real samples, such as ascorbate, urate, bilirubin, etc. Thus, the current research on H_2O_2 detection is mainly focused on electrode modifications in order to decrease the overpotential and increase the electron transfer kinetics.[27]

In conclusion, the electrochemical characterization of SAMN@DNA conjugates demonstrated that DNA immobilization on SAMNs facilitates the electron transfer between electroactive species in solution and maghemite, showing high stability and reversibility. Furthermore, a dependence of electrochemical performances of conjugates on DNA length emerged.

2.3. Electrochemical Characterization of 3D SAMN@DNA Nanobioconjugate

Above reported results suggest a synergistic interaction between nucleic acids and SAMNs, as well as an electrical

contact between the two, inferring the occurrence of charge transfer processes between DNA and the iron oxide nanoparticles. An effect of linker DNA on electrochemical properties of SAMN@DNA conjugates should also be taken into account. In order to test long range electron transfer in DNA, the electrochemical properties of SAMN@DNA metamaterial, were studied. In this case, it should be noted that SAMN clusters, inside the metamaterial framework, are well distributed and distanced (see Figures 1, S9, and S10, Supporting Information). As a consequence, DNA is responsible of the electrochemical features of the nanobioconjugate metamaterial. In term of DNA–maghemite mass ratio, the metamaterial represents an opposite situation with respect to the one- and 2D nanobioconjugates, in which DNA was a minor component. As previously described, the metamaterial nanobioconjugate is constituted of 25% DNA, 70% water, and 5% SAMNs. A CPE, prepared by mixing 55% (w/w) graphite, 30% (w/w) silicone grease, and 15% (w/w) SAMN@DNA metamaterial, was prepared and inserted in an electrochemical cell (schematically depicted in Figure S11, Supporting Information). **Figure 2** shows the cyclic voltammograms of CPE modified with the metamaterial, along with control SAMNs/CPE.

A higher capacitive current and the appearance of two cathodic (at –0.05 and –0.35 V vs SCE) and one anodic peaks (at +0.33 V vs SCE) were observed with the electrode constituted of SAMN@DNA metamaterial modified CPE. Faradic waves, which can be attributed to redox properties of nucleotidic bases, appear at very low applied potentials, when compared to examples reported in literature.[28] Furthermore, the electrode response is constant over repetitive scans, showing that the metamaterial is electrochemically stable. The proposed CP electrode modified with SAMN@DNA metamaterial was also tested for hydrogen peroxide reduction, in order to study its electrocatalytic properties. The inset of Figure 2 shows, in this context, the cyclic voltammetries of the metamaterial modified CP electrode, in the presence of increasing concentrations of H_2O_2. The material showed good sensitivity toward hydrogen peroxide. Considering that maghemite nanoparticles comprised only 0.75% of the modified CPE, the effect of DNA on the CPE elecrocatalytic properties is evident. Moreover, the absence of a conductive matrix, such as carbon paste, should further evidence the role of DNA in the long-range electron transfer. The metamaterial, as such, was inserted into the cavity of a glass electrode holder (1.35 mm diameter). Thus, a copper wire was inserted into the SAMN@DNA metamaterial, through the opposite side of the glass capillary, to create the electrical contact with the potentiostat. It is noteworthy that the system presented a low contact resistance with metal electrodes, conversely to other reports,[8b] further evidencing DNA conductivity. A representative cyclic voltammetry, acquired with the SAMN@DNA electrode, is shown in **Figure 3**, in which a broad anodic peak was observed at about +0.29 V, versus SCE, probably due to purine bases oxidation, and two cathodic peaks (at –0.150 and –0.730 V vs saturated calomel eletrode, SCE), attributable to adenine and cytosine reduction, were observed.[28] The electrode was repeatedly subjected to potential sweeps and maintained its electrochemical features up 100 cyclic voltammetry scans, revealing high stability and evidencing the reversibility of the redox events inside the DNA–SAMN framework. Furthermore, the electrode response resulted constant, if stored at 4 °C in buffer, for up to 30 days. It should be noted that, oxidation and reduction of nucleic acid bases on common electrodes are known to be irreversible and to occur at very high applied potentials.[29] Conversely, DNA immobilization on SAMNs lower electron transfer band gap and allow DNA to continuously participate at electron transfer with the electrochemical cell, evidencing that DNA, under the proper condition, can behave as electrically conductive. Finally, even if nanoparticle clusters were evenly distributed at regular distance among each other (about 100 nm), the metamaterial resulted electrically conductive and an estimate of its resistance was of 70–80 Ω cm^{-1}.

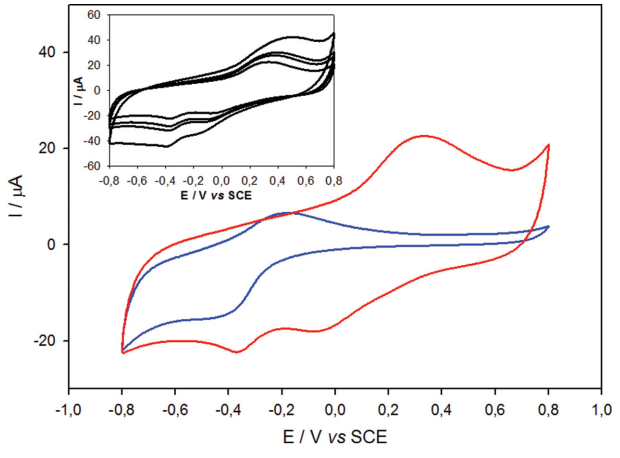

Figure 2. Cyclic voltammogramms of a CPE modified with 15% of SAMN@DNA metamaterial. Measurements were carried out in 0.1 M phosphate buffer, pH 7.0 containing 50×10^{-3} M KCl as supporting electrolyte, equilibrated in air. (Blue) CPE containing 15% SAMN; (red) CPE containing 15% SAMN@DNA metamaterial. Inset: Cyclic voltammogramms of CPE modified with 15% of SAMN@DNA metamaterial in the presence of increasing concentrations of hydrogen peroxide. Hydrogen peroxide concentrations were in the 0.0–2.0×10^{-3} M range.

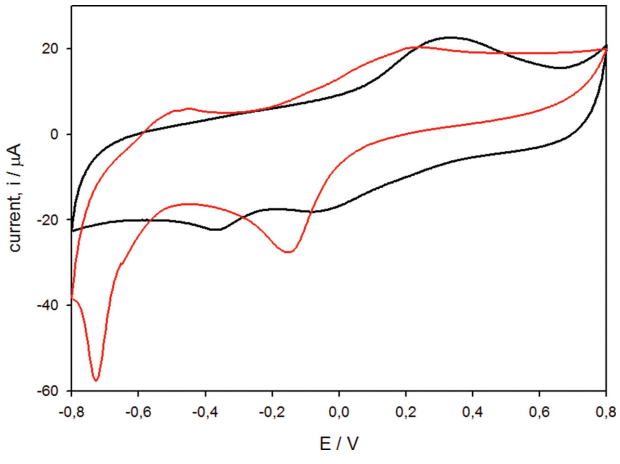

Figure 3. Cyclic voltammogramms of an electrode constituted of SAMN@DNA metamaterial. Measurements were carried out in 0.1 M phosphate buffer, pH 7.0 containing 50×10^{-3} M KCl as supporting electrolyte, equilibrated in air. (Black) CPE containing 15% SAMN; (red) SAMN@DNA metamaterial electrode.

Notwithstanding numerous and sometimes contradictory reports about DNA conductivity,[10,11a,30] these last experiments, performed on a material constituted mainly by DNA and water, give unequivocal proof of electron transfer properties of DNA, as well as, of the role of SAMNs in triggering the process. This could be related to the migration of "holes" along the DNA chain involving π-electrons of nucleotide bases, and the interaction with under-coordinated iron(III) sites on nanoparticle surface could be considered as a hole formation in the DNA chain, as it subtracts charges from the π-electron system. Charge carriers (holes) are formed at the interface between the biopolymer and SAMN surface, due to the intimate chemical, as well as electrical contact between the two conjugate components. Therefore, we suggest that the electrical properties of the metamaterial can be attributed to permanent defects (hole formation) in DNA structure induced by covalently bound maghemite nanoparticles. In particular, the overlapping of π-electron system in DNA bases may be a good candidate for long-distance charge transfer.[3]

2.4. Structural Characterization of SAMN@DNA6b Complexes

The single strand, DNA6b, characterized by a scrambled sequence, was chosen, among the tested molecules, as a reference to study intimate contact between DNA and SAMNs. This short length DNA strand can be considered as a simple organic modifier of SAMNs, and yet all the DNA structural features are available to interact with the surface iron atoms.[10] In comparison with long DNA strands, the use of short DNA sequences eliminates the presence of unbound DNA portions in the resulting conjugate, and maximizes the contact surface between the biomolecule and the nanoparticle, permitting an informative characterization. SAMN@DNA6b conjugate was first studied by TEM (**Figure 4**).

TEM microscopy images of SAMN@DNA6b complex indicated the presence of an organic matrix, forming a shell of 2 nm around iron oxide nanoparticles, characterized by a lower electron density, attributable to DNA molecules bound on SAMN surface.[31] The resulting SAMN@DNA6b complex was extremely stable and, if stored at 4 °C, DNA remained firmly bound to the iron oxide nanoparticle surface for at least 12 months. Structural characterization of SAMN@DNA6b complex was also performed by X-ray powder diffraction (XRPD) and by a superconducting quantum interference device (SQUID). The observed XRPD envelope can be ascribed to crystalline maghemite phases and the lattice parameter was determined from the refinement as a = 3.343(1) Å, and the mean size of crystalline domains was estimated, using the Scherrer equation, as 21 nm (see Figure S7, Supporting Information). The witnessed profile of the field-cooled magnetization curve indicates that the bulk properties of SAMN@DNA6b are best described as weakly interacting magnetic system, in which the through-space-interactions among nanoparticles are dipolar in nature (see Figure S8A,B, Supporting Information).

In order to obtain a deeper insight about iron oxide phase chemical and electrical interaction with DNA in the SAMN@DNA6b conjugate, zero-field and in-field ^{57}Fe Mössbauer spectroscopy was employed, identifying, among others, different valence states, types of coordination, charge distribution, and alignment of atomic magnetic moments over the crystal lattice. The measured Mössbauer spectra are shown in **Figure 5** and

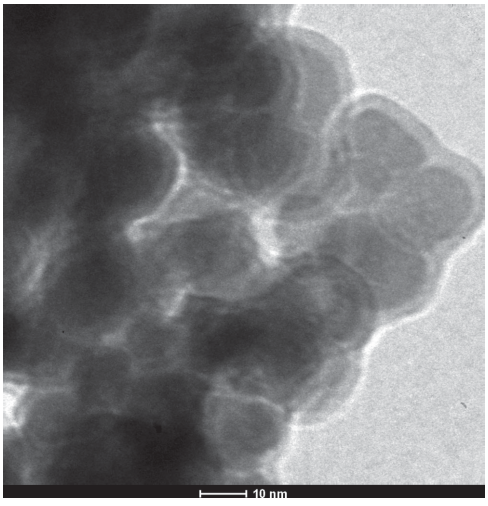

Figure 4. TEM image of maghemite nanoparticles surface-functionalized with DNA6b (SAMN@DNA6b).

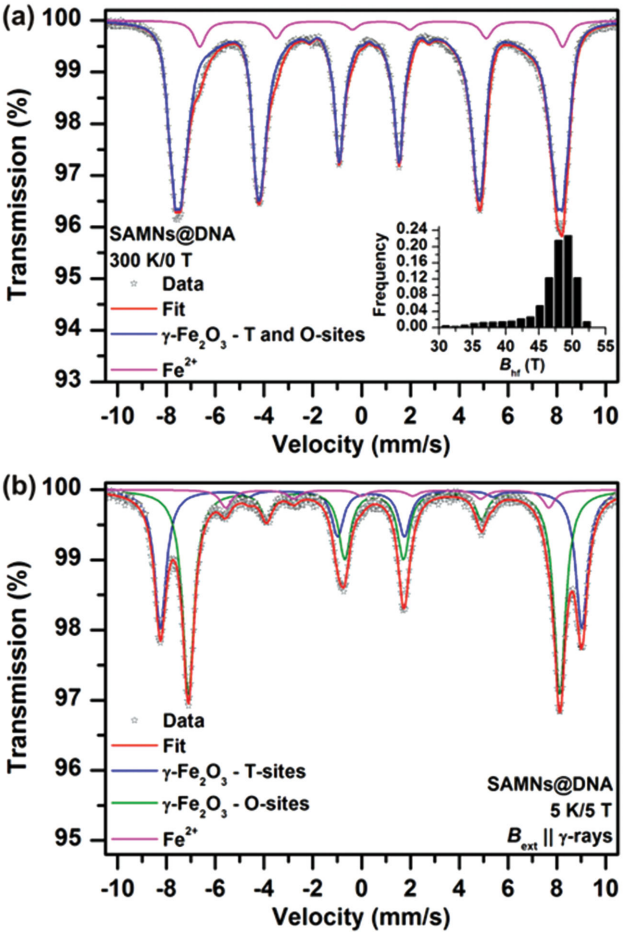

Figure 5. ^{57}Fe Mössbauer spectra of the SAMNs@DNA6b sample, recorded a) at room temperature and without an external magnetic field and b) at the temperature of 5 K and in an external magnetic field of 5 T.

values of the Mössbauer hyperfine parameters, derived from spectra fitting,[32] are listed in Table S5, Supporting Information.

At room temperature, the ^{57}Fe Mössbauer spectrum of the SAMNs@DNA6b features two magnetically split components (see Figure 5a), one sextet with the values of the Mössbauer hyperfine parameters frequently reported for γ-Fe_2O_3 with only high-spin ($S = 5/3$) Fe^{3+} ions[24,33] and the other sextet with the values of Mössbauer hyperfine parameters ascribable to the low-spin ($S = 2$) Fe^{2+} ions.[34] Owing to the nonzero value of the quadrupole splitting (ΔE_Q) parameter of the Fe^{2+} sextet, the Fe^{2+} ions most probably occupy the nanoparticle's surface (i.e., sites with octahedral coordination) where local surroundings with a nonspherical distribution of the electronic charge are expected due to symmetry breaking. For the γ-Fe_2O_3 sextet, a distribution of the hyperfine magnetic field (B_{hf}) was employed to correctly describe the non-Lorentzian profile of the Mössbauer resonant lines (see inset in Figure 5a). This finding implies that the superspins associated to the magnetic nanoparticles show collective magnetic excitations, a phenomenon often emerging in the nanoparticle systems approaching the blocking temperature (T_B).[33,35]

This behavior occurs due to thermal energy enough to cause rotation of a nanoparticle superspin around the respective easy axis of magnetization energetically favored by nanoparticle magnetic anisotropy. Thus, considering the characteristic time of the Mössbauer technique ($\approx 10^{-8}$ s), the presence of only sextet components imply that the nanoparticles experience a magnetically blocked state at room temperature with thermal energy not enough for a nanoparticle superspin to overcome the magnetic anisotropy barrier and trigger superparamagnetic fluctuations. If we assume that the nanoparticles do not magnetically interact, we can estimate the average particle size that, based on the average B_{hf}, must be larger than 15 nm, value consistent with that estimated from XRD (X-ray powder diffraction) and TEM analyses.[36]

To resolve further the Mössbauer resonant lines, the sample was cooled down to 5 K and an external magnetic field of 5 T was applied. The low-temperature in-field Mössbauer spectrum clearly shows three sextet components (see Figure 5b): (i) a sextet with the lowest isomer shift (δ) and highest B_{hf} value corresponding to the Fe^{3+} ions located in the tetrahedral (T) sites of the γ-Fe_2O_3 spinel crystal structure,[33] (ii) a sextet with a higher δ and lower B_{hf} value related to the Fe^{3+} ions occupying the octahedral (O) sites of the γ-Fe_2O_3 spinel crystal structure,[33] and (iii) a sextet with the highest δ and lowest B_{hf} value for the surface Fe^{2+} ions. Note that the spectral T (tetrahedral sites):O (octahedral sites) ratio is very close to 1:1.66 (see Table S5, Supporting Information), a value expected for ideally stoichiometric γ-Fe_2O_3 for which vacancies are present exclusively on the γ-Fe_2O_3 O-sites.[33]

Besides this, the nanoparticles in the system show, to some extent, a spin canting phenomenon when the atomic magnetic moments inside a nanoparticle are not perfectly aligned under an external magnetic field applied.[33,37] This is documented by nonzero intensity of the 2nd and 5th sextet lines for all the spectral components (Figure 5b). Thus, as the average particle size is above the threshold value at which the spin canting phenomenon significantly evolves, the nonalignment tendency may be caused by surface states having different chemical nature interacting with Fe^{3+} cations in the outermost layers of the γ-Fe_2O_3 crystal structure, most probably inducing local anisotropies. Thus, the analysis of the ^{57}Fe Mössbauer spectra confirms that on the surface of Fe_2O_3 nanoparticles Fe^{2+} states develop, in response to the linkage with DNA6b molecules. We estimated that 6% of Fe^{2+} (see Table S5, Supporting Information) corresponds approximately to 50% of the available exposed boundary iron atoms, considering that Fe^{3+} laying on SAMN surface represents about 11% of the total nanoparticle iron content, as previously reported,[20a] demonstrating an electron exchange between DNA and nanoparticles.

UV–vis spectroscopy was used to further study the SAMN@DNA6b conjugate. The interaction of DNA with SAMN surface produced an alteration of nanoparticle optical properties; both the shape and the position of maximum absorption were altered, indicating the influence of SAMN surface properties on optical characteristics and the binding occurrence (Figure S11a, Supporting Information). The electronic absorption spectrum of bare SAMNs, acquired in water, showed a wide band with a maximum at about 400 nm (Figure S11a, black line, Supporting Information) characterized by an extinction coefficient of 1520 M^{-1} cm^{-1}, expressed as Fe_2O_3 molar concentration. Differently, SAMN@DNA6b spectrum was characterized by a peak at 440 and a shoulder at 500 nm (see Figure S11a, red line, Supplemetary Information). In comparison to bare SAMNs, the observed redshift and change in the absorption envelope (shape) upon DNA6b binding is not surprising. The similar phenomenon was observed for other biomolecules, following their interaction with the nanoparticle surface, as reported in literature.[19a] We suggest that the recorded redshift in the absorption spectrum of the modified nanoparticles is due to the excitation of localized electrons from the surface modifier, in this case DNA6b, to the conduction band of the iron oxide nanoparticle,[38] in agreement with Mössbauer findings. The SAMN@DNA6b conjugate, after the washing and freeze-drying procedure, was also studied by Fourier transform IR (FTIR) spectroscopy (see Figure S11b, Supporting Information). The comparison of FTIR spectra shows that interaction of DNA6b with SAMNs led to a perturbation of the vibrational features upon DNA6b binding, including variations in the absorptions of heterocyclic bases (in the range of 1800–1500 cm^{-1}), in the vibrational coupling between the base and the sugar (1500–1250 cm^{-1}), and in the vibrational frequency of sugar-phosphate backbone (1250–900 cm^{-1}).[39] This suggests the hypothesis of a multiple point binding between DNA6b and SAMNs, in agreement with FTIR findings on other biomolecules tested in previous works.[19a,19b] Possibly, all the identified chemical groups, provided anchoring functions with respect to the surface exposed iron sites of the nanoparticles, along with an anticipated higher proclivity of the phosphate residues to chelate iron cations exposed to the bulk. The difference regarded the vibrational coupling between the base and the sugar (1500–1250 cm^{-1}) of DNA6b suggests the occurrence of a strong immobilization of the biomolecule on nanoparticle surface. Moreover, the disappearance of C–O stretching at 1050 cm^{-1}, attributable to the ribose ring, also confirmed the involvement of the sugar on the binding. The broadening of bands at 1578 and 1654 cm^{-1}, attributable to the stretching of the C=N and C=C double bonds of the aromatic heteroring

of nucleotides, indicates that aromatic bases take part at the binding with SAMN surface. Moreover, the shift of the bands corresponding to asymmetric oscillations of phosphate groups, at 1214 and 1197 cm^{-1}, evidenced their participation in the interaction with the particle surface.[40] The calculation of the intensity ratio of the symmetric and asymmetric oscillations (ν_s/ν_{as}) of phosphate group bands are 1.32 and 1.58 for DNA6b and SAMN@DNA6b respectively, confirming the participation of the phosphate groups in the formation of the bionanoconjugate.[41] Phosphate groups, in the presence of their counterions, seem to play a fundamental role in DNA charge conduction as inferred by Kratochvilova.[10] In the current case, the negative charges of the phosphate moieties were compensated by undercoordinated iron(III).

In order to shine more light into the possible binding scenarios of DNA6b to SAMNs, we tentatively modeled by density functional theory (DFT/UBP86/6-31+G*) the most probable configuration, by using an Fe(III) cation coordinated with three hydroxyl groups that may represent the surface exposed Fe metals of SAMN. There are two possible ways in which the phosphate anion can bind the surface exposed Fe, as bidentate ligand-donor or as terminal group. We found that in the presence of an arbitrary chosen base (guanosine), the most stable conformation with respect to the free base (**Figure 6**a) involves the terminal binding of the phosphate to Fe, leading to a pseudo-tetrahedral arrangement of the metal site (Figure 6b). Upon introduction of a hole in the guanosine base, hence formation of a neutral radical centre that can emerge from the aromatic N–H hydrogen-abstraction of the guanine (Figure 6c), an effective spin–spin interaction mediated by the organic backbone clearly develops between the metal centre and the newly formed radical centre, as witnessed from the spin population analyses.

In this scenario, the occurrence of an electron transfer from the organic radical to such surface exposed Fe(III) metal is possible, as observed from the Mossbauer analyses, where a fraction of Fe(III) sites of SAMNs has been found in the reduced form (namely as Fe(II)) upon interaction with DNA6b. Clearly, other electronic configurations are here possible as well, such as formation of Fe(II) sites coupled with a hole on the DNA bases.

However, although tentative, such simple model may explain how the generation of defects (holes) in the DNA bases may provide the conduction active-paths for the witnessed reversible electrochemistry of SAMN@DNA conjugates, as described earlier in their electrochemical characterization. We further tested a more complex scenario, when one surface-exposed Fe cation in the SAMN nanoparticle has been linked to one phosphate group, connecting two arbitrary chosen bases (guanosine–adenosine) (Figure 6d). In this case, a large distortion in the DNA6b structure is anticipated upon Fe binding, from the original stacked conformation of the DNA bases. Further details of the theoretical analyses are given in Tables S6–S15, Supporting Information together with the coordinate file obtained for the (a)–(d) model's geometry optimization and their frequency calculation outputs.

2.5. Discussion

The first part of the present study dealt with DNA immobilization on SAMN surface and with 1D, 2D, and 3D nanobioconjugate formation. The characteristics of SAMN@DNA conjugates depend on DNA length (in the 500–15000 bp range) and, at the same time, SAMN concentration influenced the modality of DNA immobilization, the nanoparticles loading, and, as consequence, the final architecture of the resulting conjugate. The electrochemical characteristics of SAMN@DNA conjugates were studied by EIS, cyclic voltammetry, and chronoamperometry, demonstrating that DNA immobilization facilitates the electron transfer between electroactive species in solution and maghemite nanoparticles, besides showing high stability and reversibility. Furthermore, a dependence of electrochemical performances on DNA length emerged. In particular, CPE electrodes prepared with 15% SAMN@DNA were able to catalyze the reduction of H_2O_2 at low applied potentials and, in some cases (SAMN@DNA1000bp) with good electroanalytical performances. Conversely, unbound DNA did not show any electrocatalytic activity on CPEs toward hydrogen peroxide, indicating that DNA needs to be triggered for contributing to the electrochemical performances of the electrode. The above reported experimental evidences led us to hypothesize the occurrence of a charge transfer at the interface between the biomolecule and the metal oxide nanoparticle, and the involvement of π-electrons of DNA bases, as they are the main candidates for DNA conductivity, and the conduction band of maghemite, may have a role. In this scenario, the nucleic acid behaves as a molecular wire. Thus, we forced the DNA-nanoparticle system to form a 3D nanobioconjugate, as described in the Supporting Information, namely a metamaterial, and its electrical properties were studied at a macroscopic scale. It should be reminded that water amount in the metamaterial represents 70% of the total mass, and should also contribute to material conductivity, as already reported.[10] The impressive electrochemical reversibility of the metamaterial features suggests an interpretation of the phenomenon: electrical conductivity should be correlated to highly reversible redox events on DNA bases. It should be mentioned that in the case of the metamaterial, the electrochemical system is completely different with respect to 1D and 2D nanobioconjugates, as SAMNs represent only 5% of the material mass. It is noteworthy that this metamaterial, mainly constituted by DNA and water, displayed a conductivity comparable to a carbon paste. Thus, electrochemical properties, in the absence of carbon paste matrix, further highlight the role played by SAMNs in triggering DNA conductivity. Moreover, the six base long oligonucleotide (DNA6b) was used as a probe to study the interaction at SAMN interface, and the modification of UV–vis spectrum of SAMNs, upon DNA binding, demonstrated alterations of electronic transitions and, thus, the involvement of the surface exposed iron sites, as already reported,[19a,19b,25] further suggesting the occurrence of an electron transfer between the surface modifier (DNA) and maghemite. FTIR spectroscopy confirmed the role of Fe sites on DNA binding, evidencing a wide multiple point binding, which involves all the DNA features supposed to play a role in DNA conductivity.[10] This feature depended on the covalent nature of the binding, which cannot be obtained using coated nanoparticles, or DNA immobilization through electrostatic interactions. Up to authors' knowledge, no other electrochemical study has ever been reported on DNA covalently immobilized via direct interaction with semiconductor nanoparticles. Finally, the hypothesis by

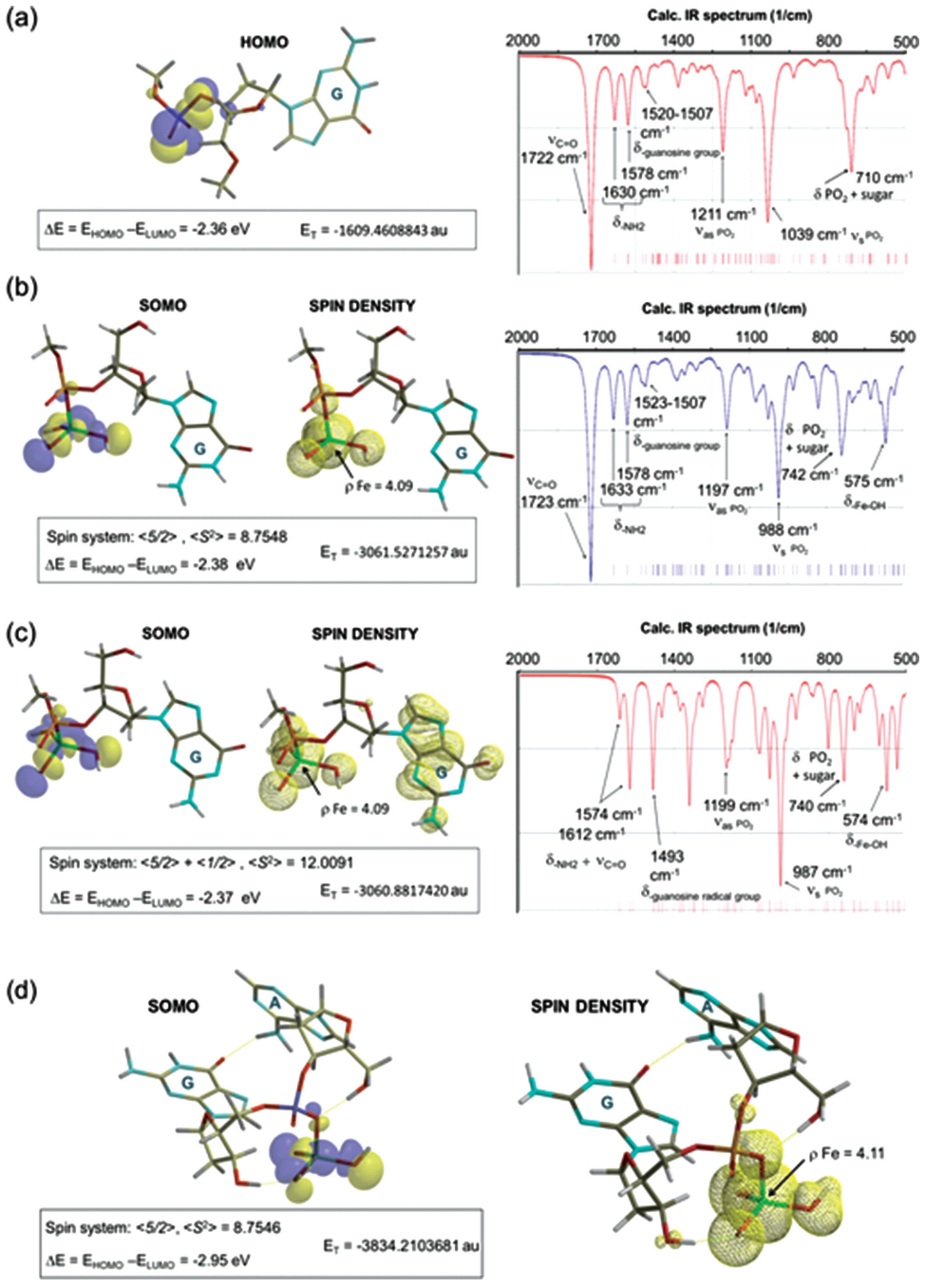

Figure 6. The DFT geometry optimized structure (RBP86/6-31+G*) of the guanosine molecule (a) and the model systems (UBP86/6-31+G*) obtained in gas-phase showing the phosphate binding to the surface exposed Fe(III) cation in SAMN@DNA materials (b–d). In the systems (a–d) the molecular charge was set to –1. In (a–c) the theoretically calculated IR spectrum at the same level of theory of the correspondent system depicted on the left is shown on the right (IR envelope drawn with Lorentzian line-width of 15 cm^{-1}). In (b–d) the spin density (ρ) isosurfaces have been drawn with 0.002 isoVal and in (a–d) the frontier orbital (HOMO, highest occupied molecular orbital, or SOMO, singly occupied molecular orbital) have been drawn at 0.032 isoVal. The thin yellow lines in (d) represent H-bonding interactions.

which SAMN binding can form electron holes on bound DNA implies that under-coordinated Fe(III) on SAMN surface accept electrons from DNA, and Mössbauer spectroscopy evidenced the presence of Fe(II) on nanoparticle surface of the SAMN@DNA conjugate, providing the experimental proof of the charge transfer occurrence at the DNA–maghemite interface, as well as of the triggering mechanism of DNA conductivity. The formation of holes in the DNA justifies all our experimental evidences, including the conductivity of the 3D nanobioconjugate (metamaterial). The development of an electron transfer from DNA to surface exposed Fe(III) on nanoparticles, as well as the generation of defects (holes) in the DNA bases was

finally modeled, tentatively, by density functional theory (DFT/UBP86/6-31+G*). The present work was not solely focused on the synthetic procedure of DNA based nanobioconjugates but aimed also to provide the proof of electrical properties of this biopolymer. This property depends on a triggering mechanism, which activates DNA electrical behavior, and SAMNs behaved as electrical trigger, as well as junction blocks for 3D structure formation.

3. Conclusions

The present report provides experimental and theoretical contribution in the debate about electrical properties of DNA, demonstrating that this biopolymer can participate at reversible electron transfer processes when properly triggered. Hybrid structures, constituted of DNA and SAMNs, were synthesized, and electrochemically characterized in a simple CPE configuration, showing peculiar electrochemical properties, not inherited from individual components, and suggesting a synergy between DNA and SAMNs. In this context, SAMNs offered the double advantage of permitting the formation of different DNA based nanobioconjugates, characterized by different architectures, and of activating electron transfer between the biopolymer and the metal oxide surface, thus triggering DNA conductivity. The triggering role of SAMNs, as well as DNA conductivity, was demonstrated by synthetizing a 3D nanobioconjugate. This macroscopic metamaterial, mainly constituted of water and DNA, is conductive and can be repeatedly subjected to cyclic voltammetries without any alteration of its electrochemical features. In addition, Mössbauer spectroscopy, showing the appearance of Fe(II) atoms on maghemite nanoparticles following nanobioconjugate formation, unequivocally witnessed the electron transfer between the biopolymer and the metal oxide. Finally, modeling by density functional theory further proved that the generation of reversible oxidation defects (holes) in DNA may provide the conduction paths for the witnessed reversible electrochemical behavior of SAMN@DNA conjugates. An effective spin–spin interaction mediated by the organic backbone probably develop between the metal centre and the newly formed radical centre, suggesting the involvement π-electrons shared by DNA bases on maghemite nanoparticles. In conclusion, the present report opens a window on electrical properties of DNA and indicates new developments of DNA based superstructures, as conductive platforms for nanoelectronics.

4. Experimental Section

Chemicals and Materials: Chemicals were purchased at the highest commercially available purity and were used without further treatment. Iron(III) chloride hexahydrate (97%), sodium borohydride ($NaBH_4$), ammonium perchlorate, and ammonium hydroxide solution (35% in water) were obtained from Aldrich (Sigma-Aldrich, Italy). Oligonucleotides, pUC-F (5' to 3': TCGCGCGTTTCGGTGATGAC), pUC-R_1 (AGCGGATAACAATTTCACAC), pUC-R_2 (TCGGAACAGGAGAGCGCACG), pUC-R_3 (GTTCCACTGAGCGTCAGACC), and pUC-R_4 (TTGGGAACCGGAGCTGAATG) were purchased from Invitrogen. The six base-long, scrambled, oligonucleotide (DNA6b) was also purchased from Invitrogen. DNAse I (deoxyribonucleate 5'-oligonucleotidohydrolase, cat. D5319) was purchased from Sigma-Aldrich (Italy). Nanoparticles (2 g L^{-1}) were suspended in MilliQ grade water (3.5 L) by treatment in an ultrasonic bath at 48 kHz, 50 W (Bransonic, mod. 221 at 48 kHz, 50 W), for at least 3 h, giving a stable colloidal suspension.

Instrumentation: Optical spectroscopy was performed in 1 cm quartz cuvettes using a Cary 50 spectrophotometer (Varian Inc., USA). FTIR spectra were acquired using a Nicolet Nexus 670 instrument (Thermo-Fisher Scientific Inc., USA). SAMN@DNA6b samples were lyophilized, homogenized with KBr powder and pelleted by an 8.0 tons hydraulic press. XRPD pattern for the SAMN@DNA6b sample was obtained at room temperature using a X´Pert PRO MPD (PANalytical, The Netherlands) instrument in Bragg–Brentano geometry with iron-filtered, Co-Kα radiation (40 kV, 30 mA, $\lambda = 0.1789$ nm) equipped with an X´Celerator detector and programmable divergence and diffracted beam antiscatter-slits. Bulk magnetic susceptibility of SAMN@DNA6b was measured by a SQUID (MPMS XL-7, Quantum Design, USA). Transmission ^{57}Fe Mössbauer spectra on SAMN@DNA6b were recorded by employing a Mössbauer spectrometer operating at a constant acceleration mode and equipped with 50 mCi ^{57}Co(Rh) source. Microscopic characterizations of SAMNs, as well as SAMN@DNA conjugates and metamaterial, were performed by TEM using a FEI Tecnai 12 microscope operating at 120 kV with a point-to-point resolution of 1.9 Å. Voltammetric experiments were carried out by a computer-controlled electrochemical workstation (PGSTAT 10, EcoChemie, The Netherlands). The standard three-electrode arrangement consisted of a SCE reference electrode (Amel, Italy), a Pt counter electrode (Amel, Italy), and CPE as working electrode.

Supporting Information

Supporting Information is available from the Wiley Online Library or from the author.

Acknowledgements

The present experimental work was partially funded by Italian Institutional Ministry grants cod. 60A06-7411 and 60A06-8055 and by CARIPARO (Cassa Risparmio di Padova e Rovigo) foundation. The authors gratefully acknowledge the support by the Operational Program Research and Development for Innovations – European Regional Development Fund (project CZ.1.05/2.1.00/03.0058) and by the Operational Program Education for Competitiveness – European Social Fund (project CZ.1.07/2.3.00/20.0155) of the Ministry of Education, Youth and Sports of the Czech Republic, and the Grant Agency of the Academy of Sciences of the Czech Republic (KAN115600801 and KAN200380801). The authors thank the electron microscopy facility of the Biology Department of Padua University.

Received: December 10, 2014
Revised: January 28, 2015
Published online: February 18, 2015

[1] O. I. Wilner, Y. Weizmann, R. Gill, O. Lioubashevski, R. Freeman, I. Willner, *Nat. Nanotechnol.* **2009**, *4*, 249.
[2] P. W. K. Rothemund, *Nature* **2006**, *440*, 297.
[3] J. Bath, A. J. Turberfield, *Nat. Nanotechnol.* **2007**, *2*, 275.
[4] a) S. Záliš, I. Kratochvílová, A. Zambova, J. Mbindyo, T. E. Mallouk, T. S. Mayer, *Eur. Phys. J. E* **2005**, *18*, 201; b) I. Kratochvílová, A. Zambova, J. Mbindyo, B. Razavi, J. Holakovský, *Mod. Phys. Lett. B* **2002**, *16*, 161; c) I. Kratochvílová, S. Nešpůrek, J. Šebera, S. Záliš, M. Pavelka, G. Wang, J. Sworakowski, *Eur. Phys. J. E* **2008**, *25*, 299;

d) I. Kratochvílová, K. Král, M. Bunček, S. Nešpůrek, T. Todorciuc, M. Weiter, J. Navrátil, B. Schneider, J. Pavluch, *Cent. Eur. J. Phys.* **2008**, *6*, 422.

[5] a) K.-H. Yoo, D. H. Ha, J.-O. Lee, J. W. Park, J. Kim, J. J. Kim, H.-Y. Lee, T. Kawai, H. Y. Choi, *Phys. Rev. Lett.* **2001**, *87*, 198102; b) G. Maruccio, P. Visconti, V. Arima, S. D'Amico, A. Biasco, E. D'Amone, R. Cingolani, R. Rinaldi, *Nano Lett.* **2003**, *3*, 479.

[6] a) X. Zhao, R. Tapec-Dytioco, W. Tan, *J. Am. Chem. Soc.* **2003**, *125*, 11474; b) G.-J. Zhang, G. Zhang, J. H. Chua, R.-E. Chee, E. H. Wong, A. Agarwal, K. D. Buddharaju, N. Singh, Z. Gao, N. Balasubramanian, *Nano Lett.* **2008**, *8*, 1066.

[7] D. Porath, A. Bezryadin, S. de Vries, C. Dekker, *Nature (London)* **2000**, *403*, 635.

[8] a) H. Nakao, H. Shiigi, Y. Yamamoto, S. Tokonami, T. Nagaoka, S. Sugiyama, T. Ohtani, *Nano Lett.* **2003**, *3*, 1391; b) H. J. Kim, Y. Roh, B. Hong, *J. Appl. Phys.* **2009**, *105*, 074302.

[9] B. Giese, *Curr. Opin. Chem. Biol.* **2002**, *6*, 612.

[10] I. Kratochvilova, K. Kral, M. Buncek, A. Viskova, S. Nespurek, A. Kochalska, T. Todorciuc, M. Weiter, B. Schneider, *Biophys. Chem.* **2008**, *138*, 3.

[11] a) R. G. Enders, D. L. Cox, R. R. P. Singh, *Rev. Mod. Phys.* **2004**, *76*, 195; b) E. B. Starikov, S. Tanaka, N. Kurita, Y. Sengok, T. Natsume, W. Wenzel, *Eur. Phys. J. E* **2005**, *18*, 437; c) M. Taniguchi, T. Kawai, *Physica E* **2006**, *33*, 1; d) H. Cohen, C. Nogues, R. Naaman, D. Porath, *Proc. Natl. Acad. Sci. USA* **2005**, *102*, 11589; e) D. Ullien, H. Cohen, D. Porath, *Nanotechnology* **2007**, *18*, 424015.

[12] D. T. Odom, E. A. Dill, J. K. Barton, *Chem. Biol.* **2000**, *7*, 475.

[13] F. Boussicault, M. Robert, *Chem. Rev.* **2008**, *108*, 2622.

[14] G. P. Triberis, M. Dimakogianni, *Recent Pat. Nanotechnol.* **2009**, *3*, 135.

[15] I. Willner, B. Willner, *Nano Lett.* **2010**, *10*, 3805.

[16] a) E. Braun, Y. Eichen, U. Sivan, G. Ben-Uoseph, *Nature (London)* **1998**, *391*, 775; b) J. Richter, M. Mertig, W. Pompe, I. Monch, H. K. Schackert, *Appl. Phys. Lett.* **2001**, *78*, 536; c) W. E. Ford, O. Harnack, A. Yasuda, J. M. Wessels, *Adv. Mater.* **2001**, *13*, 1793; d) C. F. Monson, A. T. Woolley, *Nano Lett.* **2003**, *3*, 359.

[17] a) L. Dong, T. Hollis, B. A. Connolly, N. G. Wright, B. R. Horrocks, A. Houlton, *Adv. Mater.* **2007**, *19*, 1748; b) W. U. Dittmer, F. C. Simmel, *Appl. Phys. Lett.* **2004**, *85*, 633.

[18] a) Y. Ma, J. Zhang, G. Zhang, H. He, *J. Am. Chem. Soc.* **2004**, *126*, 7079; b) H. Nakao, H. Hayashi, F. Iwata, H. Karasawa, K. Hirano, S. Sugiyama, T. Ohtani, *Langmuir* **2005**, *21*, 7945.

[19] a) M. Magro, A. Faralli, D. Baratella, I. Bertipaglia, S. Giannetti, G. Salviulo, R. Zboril, F. Vianello, *Langmuir* **2012**, *28*, 15392; b) G. Sinigaglia, M. Magro, G. Miotto, S. Cardillo, E. Agostinelli, R. Zboril, e. Bidollari, F. Vianello, *Int. J. Nanomed.* **2012**, *7*, 2249; c) D. Baratella, M. Magro, G. Sinigaglia, R. Zboril, G. Salviulo, F. Vianello, *Biosens. Bioelectron.* **2013**, *45*, 13.

[20] a) M. Magro, D. Baratella, G. Salviulo, K. Polakova, G. Zoppellaro, J. Tucek, J. Kaslik, R. Zboril, F. Vianello, *Biosens. Bioelectron.* **2014**, *52*, 159; b) M. Magro, R. Campos, D. Baratella, G. Lima, K. Hola, C. Divoky, R. Stollberger, O. Malina, C. Aparicio, G. Zoppellaro, R. Zboril, F. Vianello, *Chem. Eur. J.* **2014**, *20*, 11913.

[21] I. Langmuir, *J. Am. Chem. Soc.* **1918**, *40*, 1361.

[22] F. M. Ausubel, R. Brent, R. E. Kingston, D. D. Moore, J. G. Seidman, J. A. Smith, K. Struhl, *Current Protocols in Molecular Biology*, Wiley, Hoboken, NJ, USA **1995**.

[23] A. A. Zinchenko, F. Luckel, K. Yoshikawa, *Biophys. J.* **2007**, *92*, 1318.

[24] R. M. Cornell, U. Schwertmann, *The Iron Oxides*, Wiley, Weinheim, Germany **2003**.

[25] M. Magro, D. Baratella, N. Pianca, A. Toninello, S. Grancara, R. Zboril, F. Vianello, *Sens. Actuators B* **2013**, *176*, 322.

[26] a) J. F. Rubinson, Y. P. Kayinamura, *Chem. Soc. Rev.* **2009**, *38*, 3339; b) M. Gebala, W. Schuhmann, *Phys. Chem.* **2012**, *14*, 14933.

[27] W. Chen, S. Cai, Q. Q. Ren, W. Wen, Y. D. Zhao, *Analyst* **2012**, *137*, 49.

[28] E. Palecek, M. Bartosik, *Chem. Rev.* **2012**, *112*, 3427.

[29] S. Steenken, S. V. Jovanovic, *Am. Chem. Soc.* **1997**, *119*, 617.

[30] M. S. Xu, S. Tsukamoto, S. Ishida, M. Kimatura, Y. Arakawa, R. G. Endres, M. Shimoda, *Appl. Phys. Lett.* **2005**, *87*, 083902.

[31] J. E. Krebs, E. S. Goldstein, S. T. Kilpatrick, *Lewin's Gene XI*, Jones & Bartlett, Burlington, MA **2012**.

[32] Z. Klencsar, E. Kuzmann, A. Vertes, *J. Radioanal. Nucl. Chem.* **1996**, *210*, 105.

[33] J. Tucek, R. Zboril, D. J. Petridis, *Nanosci. Nanotechnol.* **2006**, *6*, 926.

[34] N. N. Greenwood, T. C. Gibb, *Mössbauer Spectroscopy*, Chapman and Hall, London, UK **1971**.

[35] S. Mørup, H. Tøpsoe, *Appl. Phys.* **1976**, *11*, 63.

[36] J. L. Dormann, D. Fiorani, E. Tronc, in *Advances in Chemical Physics*, Vol. *98* (Eds: I. Prigogine, S. A. Rice), Wiley, Hoboken, NJ **1997**.

[37] E. Tronc, P. Prené, J. P. Jolivet, J. L. Dormann, J. M. Grenèche, *Hyperfine Interact.* **1997**, *112*, 97.

[38] T. Rajh, J. M. Nedeljkovic, L. X. Chen, O. Poluektov, M. C. Thurnauer, *J. Phys. Chem. B* **1999**, *103*, 3515.

[39] A. G. Pershina, A. E. Sazonov, L. M. Ogorodova, *Russ. J. Bioorg. Chem.* **2009**, *35*, 607.

[40] a) H. Malonga, J. F. Neault, H. Arakawa, H. A. Tajmir-Riahi, *DNA Cell Biol.* **2006**, *25*, 63; b) H. A. Tajmir-Riahi, R. Ahmad, M. Naoui, S. Diamantoglou, *Biopolymers* **1995**, *35*, 493.

[41] a) A. A. Quameur, H. Arakaw, R. Ahmad, M. Naoui, H. A. Tajmir-Riahi, *DNA Cell Biol.* **2005**, *24*, 394; b) S. B. Dev, L. Walters, *Biopolymers* **1990**, *29*, 289.